Synergistic CO$_2$ hydrogenation over bimetallic Ru/Ni nanoparticles in ionic liquids

Muhammad I. Qadir[a], Fabiano Bernardi[b], Jackson D. Scholten[a], Daniel L. Baptista[b], Jairton Dupont[a],*

[a] Institute of Chemistry-Universidade Federal do Rio Grande do Sul-UFRGS-Av. Bento Gonçalves, 9500 Porto Alegre 91501-970, Porto Alegre, RS, Brazil
[b] Institute of Physics, UFRGS, Av. Bento Gonçalves, 9500, Porto Alegre, 91501-970, RS, Brazil

A B S T R A C T

The direct conversion of carbon dioxide to hydrocarbons is one of the key solutions to both the reduction of the greenhouse effect and the sustainable production of fuels and lubricants. Here, it is demonstrated that simple bimetallic Ru/Ni nanoparticles (NPs) (2–3 nm, Ru-rich shell, and Ni-rich core) in a hydrophobic ionic liquid (IL) promote the direct hydrogenation of CO$_2$ to light hydrocarbons (HCs) under very mild reaction conditions in a simple batch reactor. The reaction of CO$_2$ with hydrogen (1:4, 8.5 bar) at 150 °C with the Ru/Ni NPs (3:2) in bis ((trifluoromethyl)sulfonyl)amide (BMI.NTf$_2$) hydrophobic IL affords C$_2$+ hydrocarbons (79% alkanes and 16% olefins) with 5% CH$_4$ at 30% conversion. However, the reaction performed in the hydrophilic IL 1-n-butyl-3-methyl-1H-imidazol-3-ium tetrafluoroborate affords mainly CO. The catalytic hydrogenation of CO$_2$ towards HCs proceeds by a two-step process with the initial conversion of CO$_2$ into CO by reverse gas shift reaction (RWGS), followed by Fischer-Tropsch Synthesis (FTS). The bimetallic NPs have higher catalytic efficiencies than their monometallic counter- parts, owing to strong synergy between the metals. The presence of Ni in the bimetallic NPs yields a more active RWGS catalyst, and the Ru increases the FTS towards heavier HCs.

1. Introduction

The conversion of CO$_2$ into chemicals and fuels is a key component towards a resource and energy efficient future for the chemical industry [1–3]. Catalysts can combine CO$_2$-H$_2$ to create C1 units and thus provide a "greener" alternative to conventional stoichiometric reagents, resulting in high atom economy with water as the sole by-product [4,5]. In this vein, several recent breakthroughs on the activation of CO$_2$ have been recently reported for the production of chemicals [6–16]. However, for the largest applications of CO$_2$, such as for the generation of hydrocarbons, the current knowledge is in its infancy. Indeed, mimicking nature and transforming CO$_2$ as plants do is certainly one of the best solutions, but so far artificial photosynthesis is still far away from technological applications [17]. On the other hand, the transformation of CO$_2$ to methanol [18–21] or Fischer-Tropsch (FT) type processes are probably much closer to technological implementation. In the later transformation, CO$_2$ is converted into CO and water via a reverse water gas shift reaction (RWGS), and the formed CO can enter into the well-known FT technology [22] to produce clean fuels and lubricants [23]. In a recent comparative cost/benefit and energy balance addressing the

critical scientific and technical challenges that impact the economic feasibility of synthesizing jet fuel using carbon dioxide and hydrogen, the economic viability of such processes was shown [24]. Moreover, economic factor investigations associated with the use of CO$_2$ as a possible feedstock for the production of light olefins suggests that the process was close to becoming economically viable [25].

Not surprisingly, there has been a profusion of reports on the use of FT catalytic systems using CO$_2$, mainly based on iron catalysts [2,26–32]. In fact, iron based catalysts are considered to be ideally suited for CO$_2$ hydrogenation due to intrinsic WGS and RWGS activity [33]. However, these catalysts operate at high temperatures and, therefore, are quite demanding energetically and are often easily deactivated. In this vein, CO$_2$ hydrogenation has been reported with supported Ru and Ni nanoparticles at very high temperature (> 250 °C) [34]. Similarly, Ni based catalysts are also quite active for RWGS [35], but for FTS (CO) they can be relatively easily deactivated due to the migration of nickel subcarbonyl adspecies during the methanation reaction [36]. Hence, the generation of hydrocarbons from CO$_2$ hydrogenation involves a delicate balance between the RWGS (CO$_2$ partial hydrogenation) and FTS path (CO hydrogenation)[37]. It has been
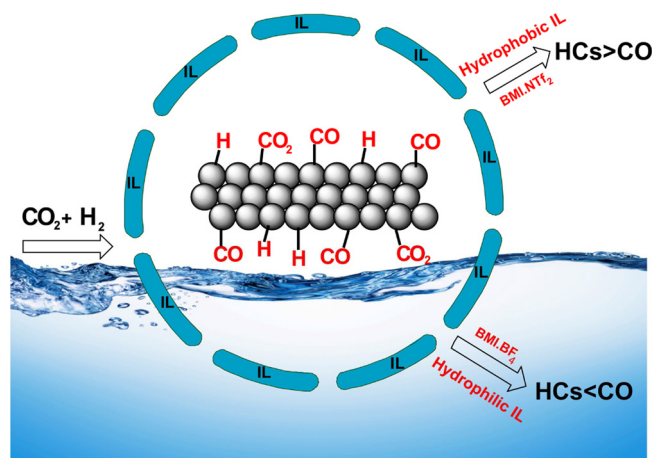
Scheme 1. Catalytic hydrogenation of CO_2 by Ru/Ni in ILs.

recently demonstrated that the association of Ru catalysts with ionic liquids (ILs) is a very promising method for the RWGS under very mild reaction conditions [12,15]. It appears that in this case, the ILs play multiple roles, such as a solvent, for catalyst stabilization, and for the expulsion of water formed in the IL catalytic phase. Moreover, ILs have also been demonstrated to be a very promising liquid support for the classical FTS using CO [38–41].

However, the Ru catalysts are usually much more active for FTS than for the RWGS and, therefore, are ultimately not suitable to perform the direct conversion of CO_2 to heavier hydrocarbons. On the other hand, Ni based catalysts are active for RWGS, but display lower reactivity towards FTS (mainly methanation) [42]. The merging of the observed IL inducing properties on RWGS and FTS of CO and designing a multiphase catalytic process that could perform the hydrogenation of CO_2 to hydrocarbons under mild reaction conditions was envisioned. The strategy was to combine the different catalytic activities of Ru and Ni towards RWGS/FTS reactions using ILs as the support (nano-container), stabilizers, and metal surface modifiers (Scheme 1). For this study, bimetallic Ru/Ni nanoparticles in an IL (BMI.NTf$_2$) were prepared and utilized, where CO_2 is highly soluble and CO is only marginally soluble [43,44], consequently shifting the equilibrium towards the formation of CO that is expulsed from the IL phase. Moreover, this IL is hydrophobic and, hence, the formed water can be easily removed from the catalytic active phase.

Here, it is reported that simple bimetallic Ru/Ni NPs in a hydrophobic IL are quite active for CO_2 hydrogenation to hydrocarbons (HCs) under unprecedented mild reaction conditions. Moreover, this represents a clear example of the synergistic catalysis over bimetallic NPs.

2. Results and discussion

2.1. Synthesis and characterisation of Ru/Ni NPs

For this study, the hydrophobic 1-butyl-3-methyl-1H-imidazol-3-ium bis((trifluoromethyl)sulfonyl)amide (BMI.NTf$_2$) IL that is well known to stabilize monometallic Ru and Ni nanoparticles was chosen [45–48]. For catalytic comparison purposes, monometallic Ni NPs of 4.9 ± 0.9 nm diameter and Ru NPs of 2.1 ± 0.5 nm diameter were also prepared in BMI.NTf$_2$ following the reported procedures [47,49]. Bimetallic Ru/Ni NPs were obtained by a simple reduction/decomposition of [Ni(COD)$_2$] and [Ru(2-methylallyl)$_2$(COD)] (COD = 1,5-cyclooctadiene) (1:3, 1:2, and 1:1 equivalents) dissolved in BMI.NTf$_2$ IL under hydrogen (8 bar, 120 °C) for 17 h. The hydrocarbons by-products were removed by simple evaporation under reduced pressure. The black colloidal suspension of NPs was analysed by Scanning transmission electron microscopy (STEM). For the Powder X-ray diffraction (PXRD), X-ray photoelectron spectroscopy (XPS) and Rutherford Backscattering Spectrometry (RBS) analysis, the Ru/Ni NPs were isolated by centrifugation. Rutherford Backscattering Spectrometry (RBS) measurements showed the Ru/Ni atomic ratio as 0.4, 1.3, and 1.5 for the Ru/Ni (1:2), Ru/Ni (4:3), and Ru/Ni (3:2) NPs, respectively (Fig. S1 of Supporting Information), indicating that some of the organometallic precursors were not incorporated into the final bimetallic materials, as already observed for other bimetallic NP syntheses in ILs [40,50]. The STEM analysis and size distribution (Fig. 1) shows the presence of irregularly shaped NPs around 2.4 ± 0.7, 2.9 ± 0.8, and 2.2 ± 0.5 nm in diameter for Ru$_1$Ni$_2$, Ru$_4$Ni$_3$, and Ru$_3$Ni$_2$ NPs respectively. This is almost similar to results obtained for monometallic Ru NPs in the same IL [47,49]. PXRD patterns of the isolated Ru/Ni NPs with different Ru/Ni concentration (% atom) ratios are shown in Fig. S2 (See supporting information), possessing a broad peak that can be ascribed as typical hexagonal close-packed (hcp) crystalline structure that is indexed as the (101) lattice plane of hcp Ru (JCPDS, No. 06-0663). The diffraction peak at 42.5° 2θ for the Ru$_1$Ni$_2$ NPs was shifted to lower diffraction angles, representing a lattice expansion originating from the substitution of the larger Ru atoms in place of the smaller Ni atoms. Similar behaviour was found for the Ni@Ru core-shell NPs, prepared by the seeding process in oleylamine solution at high temperature (200 °C) [51].

XPS measurements allowed for the identification of the chemical components present in the NPs before (as prepared case) and after the catalytic CO_2 hydrogenation reactions. The presence of C, O, F, N, and S (come from IL) were also observed beside Ru and Ni by XPS long scan spectrum measured with photon energy of 1840 eV (Fig. S9, See supporting information). Fig. 2 shows a comparison at the Ni 2p$_{3/2}$ and Ru 3d regions in the as prepared and after reaction case for each sample. The Ru 3d region is close in energy to the C 1 s region. It is possible to see an overlap between both regions. As the carbon components come
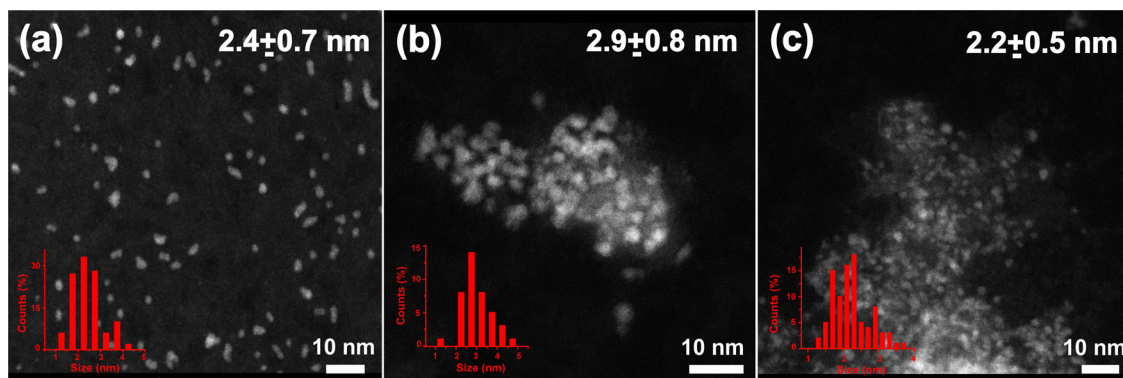

Fig. 1. STEM-HAADF images and size distribution of Ru$_1$Ni$_2$, Ru$_4$Ni$_3$, and Ru$_3$Ni$_2$ NPs prepared in BMI.NTf$_2$.
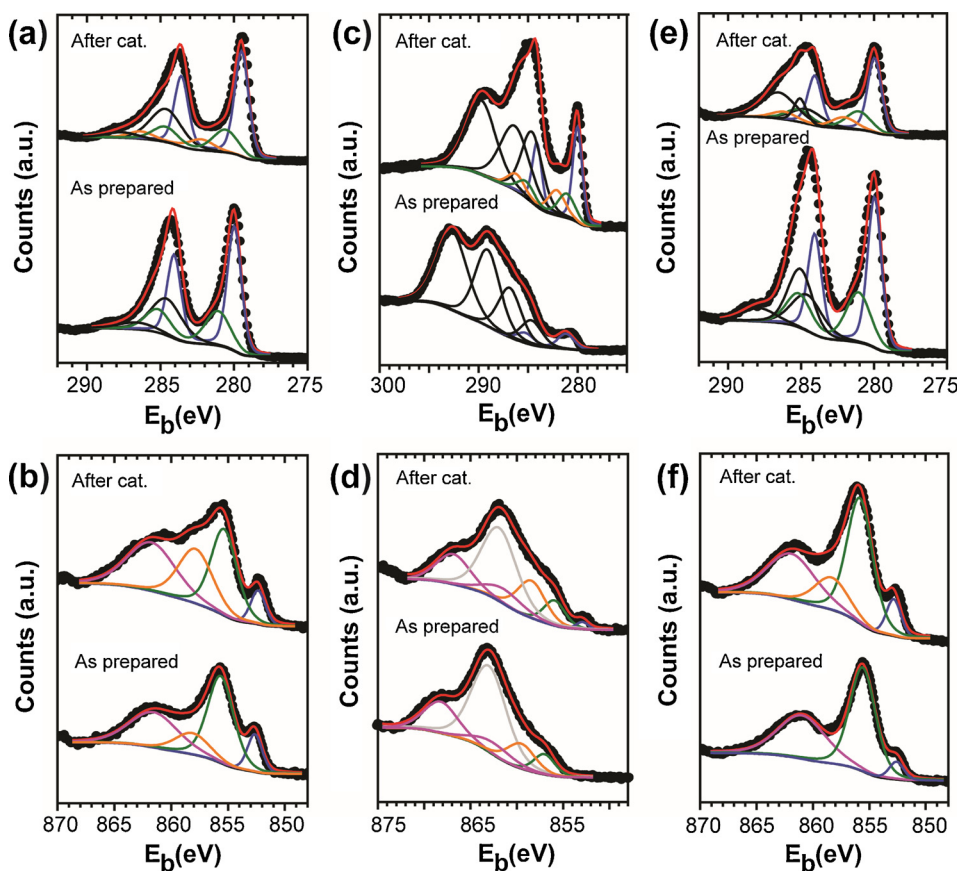
Fig. 2. Ru 3d and Ni $2p_{3/2}$ XPS spectra of the (a,b) Ru_1Ni_2, (c,d) Ru_4Ni_3, and (e,f) Ru_3Ni_2 NPs respectively, as prepared and after catalysis at $E_{ph} = 1840$ eV. Black points represent experimental points, the solid black line represents the Shirley background used, the red solid line indicates the fitting performed, and the colored line is for the chemical components. The C 1 s peaks are represented as thin solid black lines to highlight the Ru 3d components. Ru 3d (a,c,e) and Ni $2p_{3/2}$) (b,d,f) (For interpretation of the references to colour in this figure legend, the reader is referred to the web version of this article).

from different sources, it is hard to distinguish between the C 1 s and Ru 3d components. However, it is possible to identify the Ru° (blue line), Ru^{+4} (green line), and Ru^{+6} (orange line) oxidation states. The concentration (% atom) of different Ru components are represented in Table S1 (See supporting information). It is interesting to note the emergence of the Ru^{+6} component only after reaction for all samples. The Ni $2p_{3/2}$ region shows 4 distinct chemical components. It is possible to identify the presence of Ni° (blue line) and Ni^{+2} (green line) in almost all cases. Moreover, the other two components may arise due to the interaction of the IL ion pair through the F moieties to the NP surface, as already observed for Au [52]. The concentrations (% atom) of different Ni components are documented in Table S2 (see supporting information). The component represented by the grey line shows a very high binding energy value. This kind of behaviour in the XPS spectrum was already observed previously for Au nanoparticles [52].

Moreover, the change in the incident photon energy (1840 eV and 3015 eV) allowed for probing of the atomic arrangement existing in the bimetallic Ru/Ni NPs (Fig. S3). For this study, the Ni $2p_{3/2}$ and Ru $3p_{3/2}$ electronic levels were used, aiming to use similar depths probed. Table 1 shows the Ni $2p_{3/2}$/Ru $3p_{3/2}$ intensity ratio normalized by the differential cross section and incident photon flux. It is clear from Table 1 that for a given condition (as prepared and/or after reaction) there is a significant increase in the Ni $2p_{3/2}$/Ru $3p_{3/2}$ normalized ratio when increasing the probed depth (increase of the incident photon

energy from 1840 eV to 3015 eV) for all cases. This is consistent with the presence of a Ru-rich shell and Ni-rich core in all the NPs and conditions studied. This is in agreement with the surface energy, which is lower for Ru than for Ni [53], and usually observed for bimetallic NPs in which the noble metal has the tendency to populate the NP shell under reductive conditions [54,55].

It is important to note that by analysing a fixed incident photon energy of 1840 eV for NPs under different conditions (as prepared and after catalytic reaction), an increase in the Ni atomic population at the surface (increase on the Ni $2p_{3/2}$/Ru $3p_{3/2}$ ratio) for the Ru_3Ni_2 and Ru_1Ni_2 NPs was observed after the catalysis, which represents the migration of Ni atoms toward the surface during reaction. On the other hand, the Ru_4Ni_3 NPs show a small decrease in the Ni atomic population after reaction, probably due to exposure to air because Ni has the tendency to populate the NP shells under oxidation conditions [40,56]. The appearance of Ru in higher oxidation states (minor components) is not rare for bimetallic/trimetallic nanoparticles such as Pt/Ru/Ni [57]. Moreover, small nanoparticles, in particular, of Ru in organic solvents or ionic liquids are quite reactive to oxidation leading to Ru oxides [46,58].

Analysis of EXAFS (Extended X-ray Absorption Fine Structure) measurements at the Ru K edge (22,117 eV) and Ni K edge (8333 eV) was used to probe the local atomic order around Ru and Ni atoms, respectively, and then to correlate the results with the atomic

Table 1

Ni $2p_{3/2}$/Ru $3p_{3/2}$ normalized ratio obtained from the XPS analysis with two distinct incident photon energies (1840 eV and 3015 eV) of the NPs, as prepared and after catalysis.

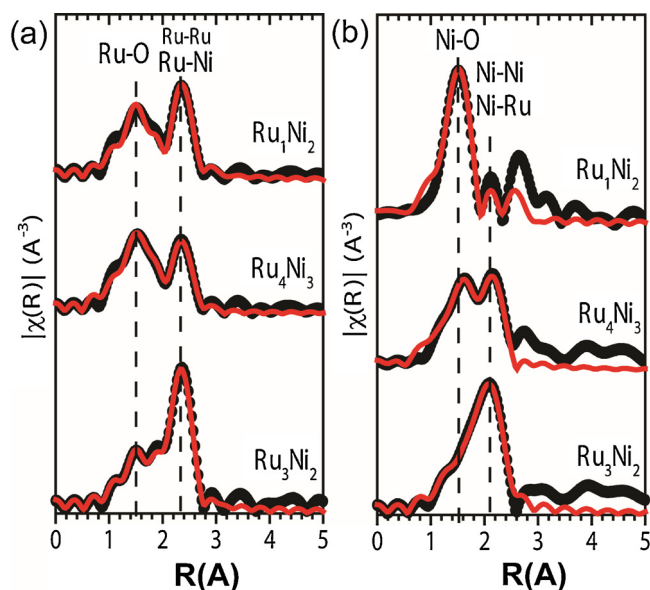| Entry	NPs	As Prep. $E_{ph} = 1840$ eV	As Prep. $E_{ph} = 3015$ eV	After Cat. $E_{ph} = 1840$ eV	After Cat. $E_{ph} = 3015$ eV
1	Ru_1Ni_2	0.24	0.40	0.64	0.90
2	Ru_4Ni_3	0.35	0.53	0.26	0.41
3	Ru_3Ni_2	0.12	0.19	0.19	0.28

Fig. 3. Comparison of the Fourier transforms (FT) of the EXAFS signal χ(k) of Ru_1Ni_2, Ru_4Ni_3, and Ru_3Ni_2 bimetallic NPs at the (a) Ru K edge and (b) Ni K edge. The black points and red lines represent the experimental data and the best fit found, respectively (For interpretation of the references to colour in this figure legend, the reader is referred to the web version of this article).

Table 2
Coordination numbers (N) obtained from the FT (Fourier transforms) analysis at the Ru K edge and Ni K edge.

NPs	N_{Ru-O}	N_{Ru-Ru}	N_{Ru-Ni}	N_{Ni-O}	N_{Ni-Ni}	N_{Ni-Ru}
Ru_3Ni_2	4.6	2.6	0.7	2.2	3.5	0.7
Ru_4Ni_3	3.8	3.8	0.9	4.0	4.4	0.9
Ru_1Ni_2	3.2	2.6	0.7	5.4	0.8	0.7

arrangement obtained from the XPS analysis. Fig. 3 shows a comparison between the as prepared samples of the FT (Fourier transforms) of the EXAFS oscillations χ(k) at the (a) Ru K edge and (b) Ni K edge. The dashed lines indicate the Ru-O, Ru-Ru, Ru-Ni, Ni-O, Ni-Ni, and Ni-Ru scattering paths used for fitting of the FT. Table 2 shows the co-ordination numbers obtained from FT analysis. For almost all cases, the N_{Ru-Ru} and N_{Ni-Ni} is significantly higher than the N_{Ru-Ni} and N_{Ni-Ru}, respectively. This is in agreement with the existence of the core-shell-like structure, as observed in the XPS analysis. The exception is the Ru_1Ni_2 NPs at the Ni K edge where N_{Ni-Ni} is approximately equal to N_{Ni-Ru}. However, in this case, the Ni-O scattering dominates the FT and the peak associated with Ni-Ni and Ni-Ru scattering is small, becoming difficult to determine the parameters associated with small uncertainty. Further more, XPS analysis (Table S2) also show that this sample has relatively more oxidized Ni, and this is mainly due to the facility that Ni is oxidized in contact with air, as already observed in other cases of Ni NPs in ionic liquids [59].These results are in agreement with the existence of NPs containing the shell of Ru and core of Ni atoms. Moreover, H_2-temperature programmed reduction (TPR) profile of Ru_1Ni_2 NPs showed a distinct peak at 464 K (Fig. S4) that probably assigned to the reduction of RuOx to Ru(0) [60]. The absence of peak around > 300 °C confirmed the absence of Ni-oxides on the surface of the NPs [61]. These observations strongly suggest that these bimetallic NPs are probably rich in Ru at the surface.

2.2. Carbon dioxide hydrogenation

Hydrogenation of CO_2 was conducted in IL (BMI.NTf$_2$) at a temperature of 150 °C. The results shown in Table 3 were obtained by

Table 3
Catalytic systems for the hydrogenation of CO_2 to HCs in ILs.[a]

Entry	NPs	Time (h)	Conv. (%)	Selectivity (%)[b]				
				CO	CH$_4$	C$_2$-C$_4$	C$_5$-C$_6$	Olefins (C$_2$-C$_4$)
1	Ru_1Ni_2	20	20	26	1	65	8	–
2	Ru_1Ni_2	60	25	0	31	55	3	11
3	Ru_4Ni_3	60	24	0	14	59	19	8
4	Ru_3Ni_2	60	30	0	5	76	3	16
5	Ru_3Ni_2[c]	60	22	47	7	7	35	4
6	Ru NPs	20	17	0	18	59	23	–
7	Ni NPs	20	5	2	4	57	37	–
8	Ru_1Ni_2[d]	20	2	–	100	–	–	–
9	–	20	–	–	–	–	–	–

[a] Reactions conditions: Catalyst 20 mg, IL (0.5 mL), CO_2/H_2 gas (1:4, 8.5 bar), 60 h and 150 °C.
[b] Selectivity of the products was calculated as equivalent amount of desired HC with respect to the total number of HCs produced.
[c] Reaction was performed in BMI-BF$_4$ hydrophilic IL.
[d] Without IL.

sealing the gas mixture (8.5 bar, H_2/CO_2 = 4:1) in a stainless-steel Fischer Porter reactor having a high-precision pressure gauge to monitor the reaction. No significant catalytic activity towards HC production was detected over pure Ni NPs (conversion 5%, Table 3, entry 7), which may be poisoned in the presence of CO_2 at low temperatures due to the formation of carbonyl groups at the surface [36]. However, on applying Ru NPs individually, the formation of HCs (hydrocarbons) was detected with 17% conversion (Table 3, entry 6). The initial induction period was observed (Fig. S5, 16 bar, H_2/CO_2 = 4:1) of 6–8 h is lower than the majority of CO_2 FTS obtained by monometallic catalysts in classical CO-FTS reactions (that can attain usually 10–15 h) [62–64], indicating that Ru is probably catalysing the Ni reduction (see below) akin to those generally observed by other bimetallic NPs containing a noble and non-noble metal component [40].

By incorporating Ni into Ru, the Ru/Ni catalysts inherited the advantages of both components, where Ru increased the total activity of Ni, and Ni tuned the selectivity towards CO and higher HCs (Table 3, entry 1) at 20 h. Interestingly, after increasing the reaction time (60 h), the activity was increased with the increase in CH$_4$ and C$_{2+}$ hydrocarbon production through FTS (Table 3, entry 2) by dominating the RWGS pathways. The reverse-water gas shift (RWGS) promoted by bi-metallic and mono-metallic Ru NPs occurs at around 80 °C in ILs that follows the formic acid production, and is much faster than the FTS in the same catalytic systems [65,66]. It is important to note that the proportion of Ru/Ni used (1:2, 1:1 and 3:2) has a profound effect not only on the conversion but also on selectivity toward HCs under standard conditions (BMI.NTf$_2$, 150 °C, 8.5 bar H_2/CO_2 (4:1), and 60 h). With the increase in Ru contents, the selectivity shifted from CH$_4$ to C$_{2+}$ hydrocarbons. It was observed that NPs containing a Ru/Ni ratio of 3:2 showed significant activity with 30% conversion toward higher HCs (Table 3, entry 4), which demonstrates a metal dilution effect [67]. Our catalytic systems demonstrated efficient activity and selectivity toward higher HCs as compared to Co-Fe [68], Ru-Co$_3$O$_4$ [69], Co-Pt/Al$_2$O$_3$ [70], Fe-RuK/TiO$_2$ [71], Co-Cu/TiO$_2$ [72], and CeO$_2$-Pt@SiO$_2$-Co [73] bimetallic catalysts, which were operated at higher temperatures (> 220 °C) and pressures (Table S3, see SI).

Since the geometric and electronic properties of metal NPs supported in ILs can be tuned by the proper choice of the IL cations and anions, along with NPs that strongly influence the residence time/diffusion of the reactants, intermediates, and products in the nano-environment [52,65,74]. Diffusion across the interface between ILs (BMI.NTf$_2$ and BMI.BF$_4$) and the catalysts surface plays an important role. Indeed, ILs form a cage around the NPs, providing an ionic nano-container environment that allows control of the diffusion of reactants,

intermediates, and products (mainly via hydrophobicity and contact ion pairs) to the catalytically active sites [50,52,74]. It was found that the hydrophobic IL (BMI.NTf$_2$) had a remarkable influence on the hydrogenation of CO_2 to heavier HCs, which not only stabilized the catalytic systems, but also repelled the formed water from the active catalytic phase of Ru/Ni NPs, hence decreasing the water gas shift reaction and increasing the FTS reaction pathways (Table 3, entry 4). Whereas, opposite phenomenon was observed when hydrogenation of CO_2 in hydrophilic BMI.BF$_4$ IL was performed that displayed a lower activity (22%) and selectivity with the production of a greater amount of CO (47%, entry 5, Table 3). This effect may be due to its hydrophilic nature that makes the formed water soluble in the IL (BMI-BF$_4$) and, therefore, may cause the reduction of the FT catalytic active surface species with the dominance of CO pathway. Moreover, the Ru can be also promoting the reduction of oxidized Ni species formed during the CO_2 reduction akin to that usually observed in bimetallic nanoparticles containing noble and non-noble metals [40]. While, the use of BMI.PF$_6$ hydrophobic IL is limited because of the generation of HF due to the partial decomposition of PF$_6^-$ anion during catalytic reactions in the presence of NPs and formed water. In all cases, high molecular weight HCs (> C$_6$) were not detected, as it is documented that during CO_2 hydrogenation a low C/H ratio is obtained due to the slow CO_2 adsorption rate on the surface of catalysts. This favours the hydrogenation of surface-adsorbed intermediates, leading to the production of lower molecular weight HCs (< C$_7$) [75].

The performance of Ru$_1$Ni$_2$ NPs versus its amount and CO_2 hydrogenation under standard conditions was also investigated (Fig. 4a). A low conversion (2%) was observed using 2 mg of catalyst. Upon increasing the catalyst amount, the conversion appears to reach a maximum at 20 mg. Moreover, the catalytic activity was also monitored at different gas pressures (Fig. 4b).

Increasing the reaction pressure showed an increased in conversion with the shifting of equilibrium of the reaction toward higher HCs. In the absence of the H$_2$/CO$_2$ gas mixture (Ru$_1$Ni$_2$, 150 °C, 60 h), the hydrogenated products and CO were not observed, which proves that the hydrogenated products were not produced from the decomposition of the IL used. ^{1}H NMR of the reaction mixture after catalysis did not show IL decomposition (Fig. S6–S7). OF note that after catalysis, maximum number of NPs were recovered by centrifugation, and the reaction was performed in the recovered IL under our standard conditions (CO$_2$/H$_2$ (4:1, 8.5 bar), 150 °C and 20 h), and we did not observe HCs formation. TEM of this recovered IL was also performed which confirm the absence of NPs in IL. Moreover, STEM-HAADF analysis (Fig. 5b) of isolated Ru$_1$Ni$_2$ NPs after CO_2 hydrogenation was also performed that revealed

no noticeable change in their size (2.39 ± 0.6 nm). In addition, CO_2 hydrogenation at different reaction conditions was also studied using Ru$_3$Ni$_2$ NPs in the BMI.NTf$_2$ IL (Table 4) in order to obtain classical FTS products. Unfortunately, under high and continuous pressure of CO_2/H$_2$, and with high concentration of H$_2$, higher HCs (> C$_6$) could not be observed, which may be related to the low CO_2 adsorption at the catalyst surface. The recyclability of the catalyst has also been studied and although no changes on the selectivity was observed, the conversion drops significantly after the second catalytic run (Fig. S8).

2.3. Surface metal segregation effect in bimetallic NPs during CO_2 hydrogenation

The surface segregation of metals in bimetallic NPs (core-shell and alloys) is quite common phenomena during catalysis [56,76] and also has become an effective and applicable tool to control surface composition and catalytic activity at the atomic level in heterogeneous catalysis, which can lead to the enrichment of one metal on the surface and other in the core [77]. It has been documented that the oxidative or reductive conditions could promote the surface segregation of 3d metals, in particular under catalytic conditions and hence changing the catalyst performance (activity and selectivity) [78].

Under reductive conditions (H$_2$ gas), the segregation of Co in Co/Pt alloy NPs [40] and Ru in Ru-Pt core-shell NPs [50] have been observed, that were prepared in ILs. When Pt-Ni NPs were studied in vacuum, H$_2$ and O$_2$ respectively, the Ni atoms always segregated to the surface of Pt-Ni NPs at 475–545 K [79]. It is important to note that the increase in Ni concentration (% atom) in the shell of our catalysts was observed after catalysis due the segregation effect studied by Synchrotron-XPS analysis at 1840 eV (Fig. 2 and also see Table 1, entries 1–3). The concentration (% atom) of segregated Ni atoms from core to shell was found in following order, Ru$_1$Ni$_2$ < Ru$_4$Ni$_3$ < Ru$_3$Ni$_2$ (Table 1). These segregated Ni atoms may play a vital role not only enhancing the RWGS pathways but also can control the selectivity of hydrocarbons. Increasing the concentration (% atom) of Ni at the surface of catalysts, an augmentation of CH$_4$ production was observed, because Ni is a well-known better methanation catalyst than Ru [36]. For example, 31%, 14% and 5% CH$_4$ was observed for Ru$_1$Ni$_2$, Ru$_4$Ni$_3$ and Ru$_3$Ni$_2$ NPs (see Table 3, entries 2–4 and Fig. 5a). Moreover, XPS measurements with a conventional X-ray source (Al K-α–hν = 1486.6 eV) for the Ru$_3$Ni$_2$ nanoparticles after 20 h of reaction showed that the normalized Ni 2p/ Ru 3p ratio in this case is 0.34, higher than 0.12 (as prepared case) and 0.19 (after 60 h of reaction), both measured with hν = 1840 eV. Besides the difference in the photon energy, it shows that the Ni segregation to
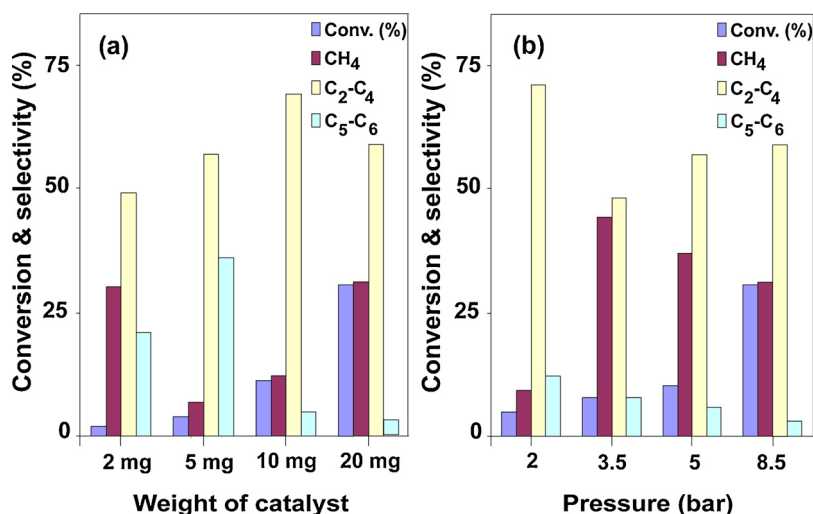

Fig. 4. Catalytic hydrogenation of CO_2 at 150 °C for 60 h in BMI.NTf$_2$ IL using Ru$_1$Ni$_2$ NPs. (a) Effect of catalyst amount under H$_2$/CO$_2$ (4:1, 8.5 bar) and (b) effect of gas pressure.
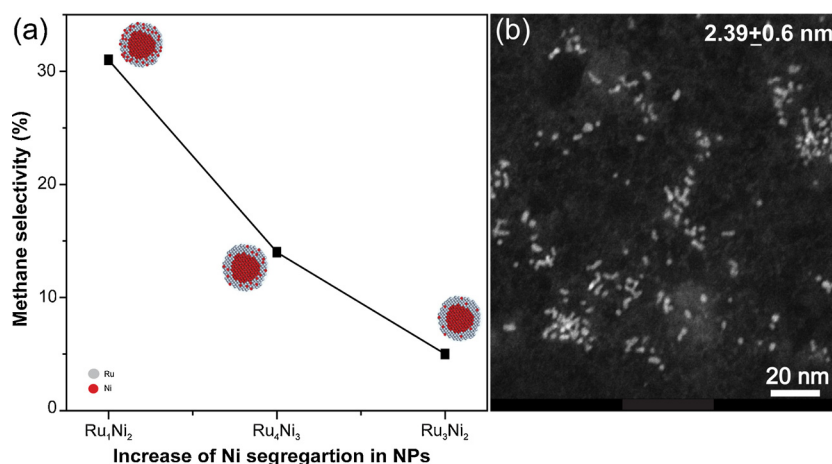
Fig. 5. (a) Surface composition of Ni in Ru/Ni NPs after catalysis vs CH$_4$ selectivity (Segregation of Ni was determined by Synchrotron XPS analysis, Table 1), and (b) STEM-HAADF analysis of Ru$_1$Ni$_2$ NPs after catalysis.

Table 4
Miscellaneous catalytic systems for the hydrogenation CO$_2$ at 150 °C in IL.[a]

Entry	NPs	P (bar)	Conv. (%)	Selectivity (%)[b]			
				CO	CH$_4$	C$_2$-C$_4$	C$_5$-C$_6$
1	Ru$_3$Ni$_2$	16	13	2	5	84	9
2	Ru$_3$Ni$_2$[c]	8.5	10	–	24	72	4
3	Ru$_3$Ni$_2$[d]	8.5	16	–	2	90	8

[a] Reactions conditions: catalyst 20 mg, BMI-NTf$_2$ (0.5 mL) and 60 h under CO$_2$/H$_2$ gas (1:4).
[b] Selectivity of the products was calculated as equivalent amount of desired hydrocarbon with respect to the total amount of hydrocarbons produced.
[c] CO$_2$/H$_2$ (1:6).
[d] Under continuous pressure of CO$_2$/H$_2$ gas (1:4).

the surface of the nanoparticles remains until 20 h of reaction, as expected akin to that observed for other bimetallic nanoparticles in ILs. A similar segregation of Ni was also studied by Synchrotron-XPS in Cu-Ni NPs under CO$_2$/H$_2$ [80].

The catalytic hydrogenation of CO$_2$ toward HC production may proceed by a two-step process with the initial conversion of CO$_2$ into CO by RWGS followed by FTS. Hence, the presence of nickel in the bimetallic NPs yields a more active RWGS catalyst and produces CO. Subsequently, activation of CO and H$_2$ proceeds preferentially on the ruthenium surface via CO* reaction with H* to form hydroxymethylene (CH*OH*) and/or via formyl (HCO*), which then dissociates to form OH*, CH*, CHx*, and COH* intermediate active species that can subsequently act as monomers and insert into chains to form higher weighted hydrocarbons [81–84].

3. Conclusions

The simple co-decomposition/reduction of Ni(0) and Ru(II) organometallic precursors in hydrophobic ILs under molecular hydrogen generates bimetallic Ru/Ni nanoparticles of 2–3 nm, with a Ru-rich shell and Ni-rich core. Under reductive conditions, a Ru-rich shell and Ni-rich core is obtained in all the samples and conditions studied, whereas after the catalytic reactions there is enrichment of Ni in the shell, owed to the migration of Ni atoms toward the surface. The NPs in the hydrophobic IL promote the direct hydrogenation of CO$_2$ to light HCs under very mild reaction conditions (150 °C, H$_2$/CO$_2$, 4:1, 8.5 bar). Thus, the reaction of CO$_2$ with hydrogen (1:4, 8.5 bar) at 150 °C with the Ru$_3$Ni$_2$ in BMI.NTf$_2$ (1-butyl-3-methyl-1*H*-imidazol-3-ium bis((trifluoromethyl) sulfonyl)amide) hydrophobic IL affords C$_2$+ hydrocarbons. However, the reaction performed in the hydrophilic IL 1-*n*-

butyl-3-methyl-1*H*-imidazol-3-ium tetrafluoborate affords mainly CO. The catalytic hydrogenation of CO$_2$ towards HCs proceeds by a two-step process with the initial conversion of CO$_2$ into CO by RWGS followed by FTS. Hence, there is a strong synergy between Ru and Ni, the presence of Ni in the bimetallic NPs yields a more active RWGS catalyst, and Ru increases the FTS towards the heavier HCs. Moreover, the Ru components also promote the reduction of oxidized Ni species of the bimetallic NPs.

4. Experimental section

4.1. General

All catalytic reactions and preparation of the nanoparticles were conducted in a stainless steel high-pressure Fischer-porter reactor. Bis (1,5-cyclooctadiene)nickel(0) and Bis(2-methylallyl)(1,5-cyclooctadiene)ruthenium(II) complexes were purchased from Sigma-Aldrich chemicals. Solvents were purified by standard procedures. BMI.NTf$_2$, BMI-BF$_4$ (1-butyl-3-methyl-1*H*-imidazol-3-ium tetrafluoroborate) and BMI.PF$_6$ (1- butyl-3-methyl-1*H*-imidazol-3-ium hexafluorophosphate) ILs were prepared from a well-known method [85]. The purified IL was dried and degassed under high vacuum at 60 °C for 2 days prior to use for the preparation of NPs and catalysis. H$_2$ (> 99.999%) and CO$_2$ (> 99.999%) were purchased from White-Martins Ltd, Brazil. XRD experiments were conducted in a D/max-3B diffractometer with Cu Kα radiation. The scans were made in the 2θ range 0–6° with a scan rate of 0.5°/min (low angle diffraction) and in the 2θ range 20–70° with a scan rate of 10°/min (wide-angle diffraction). GC-TCD analyses were run with an Agilent Micro GC System 3000 A. The conversion was monitored by pressure drop. After each catalytic reaction, ^{1}H NMR of the IL was performed and no degradation under the reaction conditions was found. A CO$_2$ hydrogenation test without IL was performed in a DRIFT cell.

4.2. Preparation of Ru/Ni NPs

The synthesis of Ru/Ni bimetallic NPs was achieved by reduction/hydrogenation of ruthenium and nickel complexes in an IL (BMI.NTf$_2$). Briefly, 0.2 mmol (55 mg) of [Ni(COD)$_2$] and 0.6 mmol (192 mg) of [Ru (methylallyl)$_2$(COD)] were added in a Fischer-porter reactor (24 mL) containing 3.0 mL of the IL in a glove box. Then, 2.0 mL of anhydrous benzene was added in order to solubilize the complexes in the IL, and this was stirred for 10 min. Benzene was then removed at reduced pressure at room temperature. Hydrogen (8 bar) was admitted to the system and was stirred intensely at room temperature for 20 min. Then, the solution was heated at 120 °C for 17 h. The reaction was cooled and

kept under reduced pressure to remove the volatiles at ambient temperature. The resulting Ru/Ni NPs were kept in IL under argon prior to use for characterizations and catalytic experiments. By changing the precursor ratio of [Ni(COD)$_2$] and [Ru(methylallyl)$_2$(COD)], Ru/Ni NPs with different compositions were prepared, with nominal Ru/Ni ratios of 3:1, 2:1, and 1:1, which, respectively, led to Ru/Ni (1:2), Ru/Ni (4:3), and Ru/Ni (3:2) NPs.

4.3. Catalytic hydrogenation of CO$_2$ by Ru/Ni NPs in ILs

The catalytic activity of the catalysts for the hydrogenation of CO$_2$ was evaluated in a stainless-steel Fischer-porter high-pressure reactor (24 mL). Typically, in a Fischer-porter reactor, 20 mg of isolated Ru/Ni NPs were dispersed into 0.5 mL of BMI.NTf$_2$ IL under argon atmosphere, and then it was quickly assembled. The reactor was kept under high vacuum for 30 min at room temperature and filled with argon. Then, the reaction reactor was flushed with a H$_2$/CO$_2$ (4:1) gas mixture to remove argon. The reactor was charged with 8.5 bars of H$_2$/CO$_2$ (4:1) and dipped into silicon oil bath that was maintained at 150 °C, and the reaction was performed. After the desired time, the reactor was cooled at room temperature and in ice bath. It was then connected to a Micro GC to analyse the gaseous products. Product selectivity was calculated as the equivalent amount of desired HC with respect to the total amount of HCs produced.

Acknowledgements

Appendix A. Supplementary data

Supplementary material related to this article can be found, in the online version, at doi:https://doi.org/10.1016/j.apcatb.2019.04.005.

References

[1] G. Centi, E.A. Quadrelli, S. Perathoner, Catalysis for CO2 conversion: a key technology for rapid introduction of renewable energy in the value chain of chemical industries, Energy Environ. Sci. 6 (2013) 1711–1731.

[2] M.V. Landau, R. Vidruk, M. Herskowitz, Sustainable production of green feed from carbon dioxide and hydrogen, ChemSusChem 7 (2014) 785–794.

[3] M. Peters, B. Kohler, W. Kuckshinrichs, W. Leitner, P. Markewitz, T.E. Muller, Chemical technologies for exploiting and recycling carbon dioxide into the value chain, ChemSusChem 4 (2011) 1216–1240.

[4] J. Klankermayer, W. Leitner, Love at second sight for CO2 and H2 in organic synthesis, Science 350 (2015) 629–630.

[5] J. Dupont, Across the Board: Jairton Dupont, ChemSusChem 8 (2015) 586–587.

[6] A.L. Girard, N. Simon, M. Zanatta, S. Marmitt, P. Goncalves, J. Dupont, Insights on recyclable catalytic system composed of task-specific ionic liquids for the chemical fixation of carbon dioxide, Green Chem. 16 (2014) 2815–2825.

[7] M. North, R. Pasquale, C. Young, Synthesis of cyclic carbonates from epoxides and CO2, Green Chem. 12 (2010) 1514–1539.

[8] K. Beydoun, T. vom Stein, J. Klankermayer, W. Leitner, Ruthenium-catalyzed direct methylation of primary and secondary aromatic amines using carbon dioxide and molecular hydrogen, Angew. Chem. Int. Ed. 42 (2013) 9554–9557.

[9] T.G. Ostapowicz, M. Schmitz, M. Krystof, J. Klankermayer, W. Leitner, Carbon dioxide as a c 1building block for the formation of carboxylic acids by formal catalytic hydrocarboxylation, Angew. Chem. Int. Ed. 52 (2013) 12119–12123.

[10] K. Beydoun, G. Ghattas, K. Thenert, J. Klankermayer, W. Leitner, Ruthenium-catalyzed reductive methylation of imines using carbon dioxide and molecular hydrogen, Angew. Chem. Int. Ed. 53 (2014) 11010–11014.

[11] L. Wu, Q. Liu, I. Fleischer, R. Jackstell, M. Beller, Ruthenium-catalysed alkoxycarbonylation of alkenes with carbon dioxide, Nat. Commun. 5 (2014) 3091–3096.

[12] Q. Liu, L.P. Wu, I. Fleischer, D. Selent, R. Franke, R. Jackstell, M. Beller, Development of a ruthenium/phosphite catalyst system for domino hydroformylation-reduction of olefins with carbon dioxide, Chem. Eur. J. 20 (2014) 6888–6894.

[13] Y. Li, X. Fang, K. Junge, M. Beller, A general catalytic methylation of amines using carbon dioxide, Angew. Chem. Int. Ed. 52 (2013) 9568–9571.

[14] Y. Li, In. Sorribes, T. Yan, K. Junge, M. Beller, Selective methylation of amines with carbon dioxide and H 2, Angew. Chem. Int. Ed. 52 (2013) 12156–12160.

[15] M. Ali, A. Gual, G. Ebeling, J. Dupont, Ruthenium-catalyzed hydroformylation of alkenes by using carbon dioxide as the carbon monoxide source in the presence of ionic liquids, ChemCatChem 6 (2014) 2224–2228.

[16] J. Artz, T.E. Müller, K. Thenert, J. Kleinekorte, R. Meys, A. Sternberg, A. Bardow, W. Leitner, Sustainable conversion of carbon dioxide: an integrated review of catalysis and life cycle assessment, Chem. Rev. 118 (2018) 434–504.

[17] V. Balzani, G. Bergamini, P. Ceroni, Light: a very peculiar reactant and product, Angew. Chem. Int. Ed. 54 (2015) 11320–11337.

[18] G.A. Olah, Beyond oil and gas: the methanol economy, Angew. Chem. Int. Ed. 44 (2005) 2636–2639.

[19] D. Mignarda, M. Sahibzadab, H.M. Duthiec, H.W. Whittington, Methanol synthesis from flue-gas CO2 and renewable electricity: a feasibility stud, Int. J. Hydrogen Energy 28 (2003) 455–464.

[20] G.A. Olah, A. Goeppert, G.K.S. Prakash, Chemical recycling of carbon dioxide to methanol and dimethyl ether: from greenhouse gas to renewable, environmentally carbon neutral fuels and synthetic hydrocarbons, J. Org. Chem. 74 (2009) 487–498.

[21] P. Vibhatavata, J.-M. Borgard, M. Tabarant, D. Bianchi, C. Mansilla, Chemical recycling of carbon dioxide emissions from a cement plant into dimethyl ether, a case study of an integrated process in france using a reverse water gas shift (rwgs) step, Int. J. Hydrogen Energy 38 (2013) 6397–6405.

[22] D.M. Drab, H.D. Willauer, M.T. Olsen, R. Ananth, G.W. Mushrush, J.W. Baldwin, D.R. Hardy, F.W. Williams, Hydrocarbon synthesis from Carbon Dioxide and hydrogen: a two-step process, Energ. Fuels 27 (2013) 6348–6354.

[23] J. Wei, Q. Ge, R. Yao, Z. Wen, C. Fang, L. Guo, H. Xu, J. Sun, Directly converting CO2 into a gasoline fuel, Nat. Commun. 8 (2017) AN15174.

[24] H.D. Willauer, D.R. Hardy, K.R. Schultz, F.W. Williams, The feasibility and current estimated capital costs of producing jet fuel at sea using carbon dioxide and hydrogen, J. Ren. Sustain. Energy 4 (2012) 033111.

[25] E.A. Quadrelli, G. Centi, J.-L. Duplan, S. Perathoner, Carbon dioxide recycling: emerging large-scale technologies with industrial potential, ChemSusChem 4 (2011) 1194–1215.

[26] M.K. Gnanamani, G. Jacobs, H.H. Hamdeh, W.D. Shafer, B.H. Davis, Fischer–tropsch synthesis: mössbauer investigation of iron containing catalysts for hydrogenation of carbon dioxide, Catal. Today 207 (2013) 50–56.

[27] R. Satthawong, N. Koizumi, C. Song, P. Prasassarakich, Comparative study on CO2 hydrogenation to higher hydrocarbons over Fe-based bimetallic catalysts, Top. Catal. 57 (2013) 588–594.

[28] F. Ding, A. Zhang, M. Liu, X. Guo, C. Song, Effect of SiO2-coating of FeK/Al2O3 catalysts on their activity and selectivity for CO2 hydrogenation to hydrocarbons, RSC Adv. 4 (2014) 8930.

[29] X. Su, J. Zhang, S. Fan, Q. Ma, T.-S. Zhao, Effect of preparation of Fe–Zr–K catalyst on the product distribution of CO2hydrogenation, RSC Adv. 5 (2015) 80196–80202.

[30] R.E. Owen, J.P. O'Byrne, D. Mattia, P. Plucinski, S.I. Pascu, M.D. Jones, Promoter effects on iron-silica fischer-tropsch nanocatalysts: conversion of carbon dioxide to lower olefins and hydrocarbons at atmospheric pressure, ChemPlusChem 78 (2013) 1536–1544.

[31] R.W. Dorner, D.R. Hardy, F.W. Williams, H.D. Willauer, Heterogeneous catalytic CO2 conversion to value-added hydrocarbons, Synth. Lect. Energy Environ. Technol. Sci. Soc. 3 (2010) 884.

[32] M. Al-Dossary, A.A. Ismail, J.L.G. Fierro, H. Bouzid, S.A. Al-Sayari, Effect of Mn loading onto MnFeO nanocomposites for the CO2 hydrogenation reaction, Appl. Catal., B Envir. 165 (2015) 651–660.

[33] D.S. Newsome, The water-gas shif reaction, Cat. Rev. - Sci. Eng. 21 (1980) 275–318.

[34] M.K. Gnanamani, G. Jacobs, R.A. Keogh, W.D. Shafer, D.E. Sparks, S.D. Hopps, G.A. Thomas, B.H. Davis, Fischer-Tropsch synthesis: Effect of pretreatment conditions of cobalt on activity and selectivity for hydrogenation of carbon dioxide, Appl. Catal. A Gen. 499 (2015) 39–46.

[35] P.C. Zonetti, S. Letichevsky, A.B. Gaspar, E.F. Sousa-Aguiar, L.G. Appel, The NixCe0.75Zr0.25 − xO2 solid solution and the RWGS, Appl. Catal. A Gen. 475 (2014) 48–54.

[36] M. Agnelli, M. Kolb, C. Mirodatos, CO hydrogenation on a nickel catalyst, J. Catal. 148 (1994) 9–21.

[37] M.S. Spencer, On the activation energies of the forward and reverse water-gas shift reaction, Catal. Lett. 32 (1995) 9–13.

[38] M. Scariot, D.O. Silva, J.D. Scholten, G. Machado, S.R. Teixeira, M.A. Novak, G. Ebeling, J. Dupont, Cobalt nanocubes in ionic liquids: synthesis and properties, Angew. Chem. Int. Ed. 47 (2008) 9075–9078.

[39] D.O. Silva, J.D. Scholten, M.A. Gelesky, S.R. Teixeira, A.C.B. Dos Santos, E.F. Souza-Aguiar, J. Dupont, Catalytic gas-to-Liquid processing using cobalt nanoparticles dispersed in imidazolium ionic liquids, ChemSusChem 1 (2008) 291–294.

[40] D.O. Silva, L. Luza, A. Gual, D.L. Baptista, F. Bernardi, M.J.M. Zapata, J. Morais, J. Dupont, Straightforward synthesis of bimetallic Co/Pt nanoparticles in ionic liquid: atomic rearrangement driven by reduction-sulfidation processes and Fischer-Tropsch catalysis, Nanoscale 6 (2014) 9085–9092.

[41] A. Gual, C. Godard, S. Castillon, D. Curulla-Ferre, C. Claver, Colloidal Ru, Co and Fe-nanoparticles. Synthesis and application as nanocatalysts in the Fischer-Tropsch process, Catal. Today 183 (2012) 154–171.

[42] H. Schulz, Short history and present trends of Fischer–Tropsch synthesis, Appl. Catal. A Gen. 186 (1999) 3–12.

[43] J.L. Anthony, J.L. Anderson, E.J. Maginn, J.F. Brennecke, Anion effects on gas solubility in ionic liquids, J. Phys. Chem. B 109 (2005) 6366–6374.

[44] Z. Lei, C. Dai, B. Chen, Gas solubility in ionic liquids, Chem. Rev. 114 (2014) 1289–1326.

[45] P. Migowski, G. Machado, S.R. Texeira, M.C.M. Alves, J. Morais, A. Traverse, J. Dupont, Synthesis and characterization of nickel nanoparticles dispersed in imidazolium ionic liquids, Phys. Chem. Chem. Phys. 9 (2007) 4814–4821.

[46] E.T. Silveira, A.P. Umpierre, L.M. Rossi, G. Machado, J. Morais, G.V. Soares, I.L.R. Baumvol, S.R. Teixeira, P.F.P. Fichtner, J. Dupont, The partial hydrogenation of benzene to cyclohexene by nanoscale ruthenium catalysts in imidazolium ionic liquids, Chem. Eur. J. 10 (2004) 3734–3740.

[47] M.H.G. Prechtl, M. Scariot, J.D. Scholten, G. Machado, S.R. Teixeira, J. Dupont, Nanoscale ru(0) particles: arene hydrogenation catalysts in imidazolium ionic liquids, Inorg. Chem. 47 (2008) 8995–9001.

[48] T. Gutel, C.C. Santini, K. Philippot, A. Padua, K. Pelzer, B. Chaudret, Y. Chauvin, J.-M. Basset, Organized 3D-alkyl imidazolium ionic liquids could be used to control the size of in situ generated ruthenium nanoparticles? J. Mater. Chem. 19 (2009) 3624–3631.

[49] M.H.G. Prechtl, P.S. Campbell, J.D. Scholten, G.B. Fraser, G. Machado, C.C. Santini, J. Dupont, Y. Chauvin, Imidazolium ionic liquids as promoters and stabilising agents for the preparation of metal(0) nanoparticles by reduction and decomposition of organometallic complexes, Nanoscale 2 (2010) 2601–2606.

[50] A. Weilhard, G. Abarca, J. Viscardi, M.H.G. Prechtl, J.D. Scholten, F. Bernardi, D.L. Baptista, J. Dupont, Challenging thermodynamics: hydrogenation of benzene to 1,3-cyclohexadiene by ru@pt nanoparticles, Chemcatchem 9 (2017) 204–211.

[51] G. Chen, S. Desinan, R. Nechache, R. Rosei, F. Rosei, D. Ma, Bifunctional catalytic/magnetic Ni@Ru core-shell nanoparticles, Chem. Commun. (Camb.) 47 (2011) 6308–6310.

[52] L. Luza, C.P. Rambor, A. Gual, J. Alves Fernandes, D. Eberhardt, J. Dupont, Revealing hydrogenation reaction pathways on naked gold nanoparticles, ACS Catal. 7 (2017) 2791–2799.

[53] A.V. Ruban, H.L. Skriver, J.K. Nørskov, Surface segregation energies in transition-metal alloys, Phys. Rev. B 59 (1999) 15990–16000.

[54] L. Hanbin, F. Adrian, Z.J. Xu, Surface Segregation in Bimetallic Nanoparticles: a critical issue in electrocatalyst engineering, Small 11 (2015) 3221–3246.

[55] S.A. Kumar, X. Qiang, Synergistic catalysis over bimetallic alloy nanoparticles, ChemCatChem 5 (2013) 652–676.

[56] F. Tao, M.E. Grass, Y.W. Zhang, D.R. Butcher, F. Aksoy, S. Aloni, V. Altoe, S. Alayoglu, J.R. Renzas, C.K. Tsung, Z.W. Zhu, Z. Liu, M. Salmeron, G.A. Somorjai, Evolution of structure and chemistry of bimetallic nanoparticle catalysts under reaction conditions, J. Am. Chem. Soc. 132 (2010) 8697–8703.

[57] K.-W. Park, J.-H. Choi, B.-K. Kwon, S.-A. Lee, Y.-E. Sung, H.-Y. Ha, S.-A. Hong, H. Kim, A. Wieckowski, Chemical and electronic effects of ni in pt/ni and pt/ru/ni alloy nanoparticles in methanol electrooxidation, J. Phys. Chem. B 106 (2002) 1869–1877.

[58] O. Vidoni, K. Philippot, C. Amiens, B. Chaudret, O. Balmes, J.O. Malm, J.O. Bovin, F. Senocq, M.J. Casanove, Novel, spongelike ruthenium particles of controllable size stabilized only by organic solvents, Angew. Chem. Int. Ed. 38 (1999) 3736–3738.

[59] Md.S. KI, F. Bernardi, G. Abarca, D.L. Baptista, M.J. Leite Santos, L. Fernandez Barquin, J. Dupont, I. de Pedro, Tuning the structure and magnetic behavior of Ni-Ir-based nanoparticles in ionic liquids, Phys. Chem. Chem. Phys. 20 (2018) 10247–10257.

[60] A. Song, G. Lu, Enhancement of Pt–Ru catalytic activity for catalytic wet air oxidation of methylamine via tuning the Ru surface chemical state and dispersion by Pt addition, RSC Adv. 4 (2014) 15325–15331.

[61] E. Zacharaki, P. Beato, R.R. Tiruvalam, K.J. Andersson, H. Fjellvåg, A.O. Sjåstad, From colloidal monodisperse nickel nanoparticles to well-defined Ni/Al2O3 model catalysts, Langmuir 33 (2017) 9836–9843.

[62] B.C. Enger, A. Holmen, Nickel and Fischer-Tropsch Synthesis, Catal. Rev. 54 (2012) 437–488.

[63] R.L. Varma, N.N. Bakhshi, J.F. Mathews, S.H. Ng, Induction periods for synthesis of hydrocarbons from syngas over metal/zeolite catalysts using a two stage process, Appl. Catal. A Gen. 32 (1987) 191–201.

[64] R.L. Varma, N.N. Bakhshi, J.F. Mathews, S.H. Ng, Performance of dual-reactor system for conversion of syngas to aromatic-containing hydrocarbons, Ind. Eng. Chem. Res. 26 (1987) 183–188.

[65] M.I. Qadir, A. Weilhard, J.A. Fernandes, I. de Pedro, B.J.C. Vieira, J.C. Waerenborgh, J. Dupont, Selective carbon dioxide hydrogenation driven by ferromagnetic rufe nanoparticles in ionic liquids, ACS Catal. 8 (2018) 1621–1627.

[66] A. Weilhard, M.I. Qadir, V. Sans, J. Dupont, Selective CO2 hydrogenation to formic acid with multifunctional ionic liquids, ACS Catal. (2018) 1628–1634.

[67] K.L. Luska, A. Bordet, S. Tricard, I. Sinev, W. Grünert, B. Chaudret, W. Leitner, Enhancing the catalytic properties of ruthenium nanoparticle-SILP catalysts by dilution with iron, ACS Catal. 6 (2016) 3719–3726.

[68] M.K. Gnanamani, G. Jacobs, H.H. Hamdeh, W.D. Shafer, F. Liu, S.D. Hopps, G.A. Thomas, B.H. Davis, Hydrogenation of carbon dioxide over Co–Fe bimetallic catalysts, ACS Catal. 6 (2016) 913–927.

[69] Y. Zhu, S. Zhang, Y. Ye, X. Zhang, L. Wang, W. Zhu, F. Cheng, F. Tao, Catalytic conversion of carbon dioxide to methane on ruthenium–cobalt bimetallic nanocatalysts and correlation between surface chemistry of catalysts under reaction conditions and catalytic performances, ACS Catal. 2 (2012) 2403–2408.

[70] R.W. Dorner, D.R. Hardy, F.W. Williams, B.H. Davis, H.D. Willauer, Influence of gas feed composition and pressure on the catalytic conversion of co2 to hydrocarbons using a traditional cobalt-based fischer − tropsch catalyst, Energ. Fuels 23 (2009) 4190–4195.

[71] U. Rodemerck, M. Holeňa, E. Wagner, Q. Smejkal, A. Barkschat, M. Baerns, Catalyst development for CO2 hydrogenation to fuels, ChemCatChem 5 (2013) 1948–1955.

[72] Z. Shi, H. Yang, P. Gao, X. Li, L. Zhong, H. Wang, H. Liu, W. Wei, Y. Sun, Direct conversion of CO2 to long-chain hydrocarbon fuels over K–promoted CoCu/TiO2 catalysts, Catal. Today 311 (2017) 65–73.

[73] C. Xie, C. Chen, Y. Yu, J. Su, Y. Li, G.A. Somorjai, P. Yang, Tandem catalysis for CO2 hydrogenation to C2–C4 hydrocarbons, Nano Lett. 17 (2017) 3798–3802.

[74] L. Luza, C.P. Rambor, A. Gual, F. Bernardi, J.B. Domingos, T. Grehl, P. Brüner, J. Dupont, catalytically active membranelike devices: Ionic Liquid Hybrid organosilicas decorated with palladium nanoparticles, ACS Catal. 6 (2016) 6478–6486.

[75] A.L. Kustov, A.M. Frey, K.E. Larsen, T. Johannessen, J.K. Nørskov, C.H. Christensen, CO methanation over supported bimetallic Ni–Fe catalysts: from computational studies towards catalyst optimization, Appl. Catal. A Gen. 320 (2007) 98–104.

[76] K. Mori, T. Sano, H. Kobayashi, H. Yamashita, Surface engineering of a supported pdag catalyst for hydrogenation of co2 to formic acid: elucidating the active pd atoms in alloy nanoparticles, J. Am. Chem. Soc. 140 (2018) 8902–8909.

[77] F. Tao, M.E. Grass, Y. Zhang, D.R. Butcher, J.R. Renzas, Z. Liu, J.Y. Chung, B.S. Mun, M. Salmeron, G.A. Somorjai, Reaction-Driven Restructuring of Rh-Pd and Pt-Pd Core-Shell Nanoparticles, Science 322 (2008) 932–934.

[78] H. Liao, A. Fisher, Z.J. Xu, Surface Segregation in Bimetallic Nanoparticles: A Critical Issue in Electrocatalyst Engineering, Small 11 (2015) 3221–3246.

[79] M. Ahmadi, F. Behafarid, C. Cui, P. Strasser, B.R. Cuenya, Long-range segregation phenomena in shape-selected bimetallic nanoparticles: chemical state effects, ACS Nano 7 (2013) 9195–9204.

[80] L. Pielsticker, I. Zegkinoglou, N.J. Divins, H. Mistry, Y.-T. Chen, A. Kostka, J.A. Boscoboinik, B.R. Cuenya, Segregation Phenomena in Size-Selected Bimetallic CuNi Nanoparticle Catalysts, J. Phys. Chem. B 122 (2018) 919–926.

[81] D. Hibbitts, E. Dybeck, T. Lawlor, M. Neurock, E. Iglesia, Preferential activation of CO near hydrocarbon chains during Fischer–Tropsch synthesis on Ru, J. Catal. 337 (2016) 91–101.

[82] Z.-P. Liu, P. Hu, A New Insight into Fischer − Tropsch Synthesis, J. Am. Chem. Soc. 124 (2002) 11568–11569.

[83] S. Shetty, R.A. van Santen, CO dissociation on Ru and Co surfaces: The initial step in the Fischer–Tropsch synthesis, Catal. Today 171 (2011) 168–173.

[84] M. Pachecka, J.M. Sturm, C.J. Lee, F. Bijkerk, Adsorption and dissociation of CO(2) on Ru(0001), J. Phys. Chem. C 121 (2017) 6729–6735.

[85] C.C. Cassol, G. Ebeling, B. Ferrera, J. Dupont, A simple and practical method for the preparation and purity determination of halide-free imidazolium ionic liquids, Adv. Synth. Catal. 348 (2006) 243–248.